Multi-pose Fusion for Autonomous Polycrystalline Material Decomposition in Hyperspectral Neutron Tomography

Diyu Yang[1], Mohammad Samin Nur Chowdhury[1], Shimin Tang[2], Singanallur V. Venkatakrishnan[3], Hassina Z. Bilheux[2], Gregery T. Buzzard[4], and Charles A. Bouman[1]

[1]School of Electrical and Computer Engineering, Purdue University, West Lafayette, IN 47907, USA
[2]Neutron Scattering Division, Oak Ridge National Laboratory, Oak Ridge, TN 37831, USA
[3]Electrical and Engineering Infrastructure Division, ORNL, Oak Ridge, TN 37830, USA
[4]Department of Mathematics, Purdue University, West Lafayette, IN 47907, USA.

2024 58th Asilomar Conference on Signals, Systems, and Computers | 979-8-3503-5405-8/24/$31.00 ©2024 IEEE | DOI: 10.1109/IEEECONF60004.2024.10942621

***Abstract*—Hyperspectral neutron computed tomography (HSnCT) is an effective technique for characterizing polycrystalline material samples. A typical scan involves making multiple HS projection measurements by rotating the sample about a single axis and using a standard algorithm for tomographic reconstruction. Recently, an autonomous polycrystalline material decomposition (APMD) algorithm was proposed to obtain accurate 3D reconstruction of the different materials or crystallographic phases in the object. However, for objects with complex compositions and shapes, using data from a single rotation axis may result in reconstructions with significant noise and inaccuracies in the material decomposition. In this paper, we present a multi-pose reconstruction algorithm to produce a single reconstruction from HSnCT data corresponding to multiple poses of the object. Our algorithm extends previous APMD work to incorporate hyperspectral neutron measurements from multiple poses, utilizing the Multi-Agent Consensus Equilibrium (MACE) framework to integrate projections from different rotation axes into a single reconstruction. We apply our method to simulated data and demonstrate that multi-pose APMD achieves significantly improved material decomposition accuracy compared to single-pose APMD.**

I. Introduction

Hyperspectral neutron computed tomography (HSnCT) is a powerful technique that enables 3D non-destructive imaging of critical material properties such as crystallographic phases [1] and isotopic compositions [2]. The typical workflow involves positioning the sample in the path of a hyperspectral neutron beam, rotating the sample about a single axis, and capturing projections with a time-of-flight (ToF) detector at each orientation. The baseline method to get a reconstruction from such data is to simply process each spectral/ToF bin independently using the Filtered Back Projection (FBP) algorithm, followed by a HS segmentation algorithm to separate the different materials/phases in the sample. However, this method is computationally expensive because of the presence of a large number of spectral bins (of the order of a few thousand) and results in inaccurate reconstructions due to the low SNR inherent in typical HSnCT data.

In order to address the high computational burden and low SNR associated with the standard workflows for HSnCT, various dimensionality reduction approaches have been developed [3], [4], [5], [6]. Notably, an autonomous polycrystalline material decomposition (APMD) algorithm has been proposed in [6], which simplifies the hyperspectral data analysis by employing a subspace extraction technique. This technique transforms high-dimensional hyperspectral projections into lower-dimensional subspace projections, which are then reconstructed using model-based iterative reconstruction (MBIR) methods [7]. These low-dimensional subspace reconstructions are then used to estimate the material-specific linear attenuation coefficients (also referred to as μ-spectra). Final material decomposition is performed using the estimated μ-spectra. However, for objects with complex shapes and compositions, even APMD can result in reconstructions with artifacts. In such cases, more accurate material decomposition could, in principle be achieved by collecting hyperspectral neutron projections corresponding to multiple rotation axes (or poses) of the object, and then performing a multi-pose reconstruction similar to what has been demonstrated in X-ray cone-beam CT [8].

In this paper, we build on the ideas of APMD [6] and Multi-pose Fusion [8], and propose a multi-pose APMD algorithm. As shown in Figure 1, the proposed algorithm first transforms the hyperspectral projections into material projections and then employs the multi-agent consensus equilibrium (MACE) [9] to fit the material projections from multiple poses, where the data fidelity from each pose is promoted with a novel MACE agent called a conjugate proximal map. The resulting algorithm has a simple modular implementation using standard CT reconstruction software. Our results on simulated data

This manuscript has been authored by UT-Battelle, LLC, under contract DE-AC05-00OR22725 with the US Department of Energy (DOE). The US government retains and the publisher, by accepting the article for publication, acknowledges that the US government retains a nonexclusive, paid-up, irrevocable, worldwide license to publish or reproduce the published form of this manuscript, or allow others to do so, for US government purposes. DOE will provide public access to these results of federally sponsored research in accordance with the DOE Public Access Plan (http://energy.gov/downloads/doe-public-access-plan).

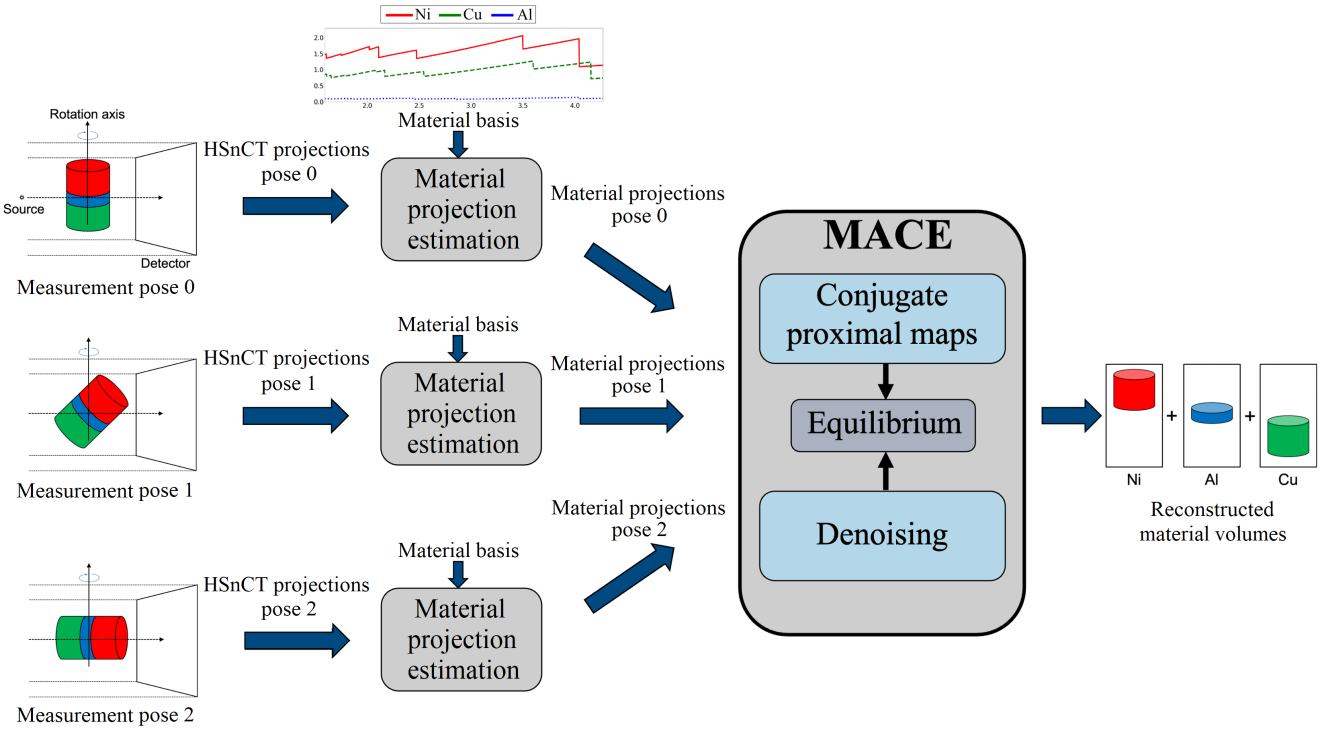

Fig. 1: Overview of multi-pose APMD algorithm. Multiple sets of hyperspectral projections are acquired from different poses of the same object. For illustration, the object is made of three materials - Nickel (red), Aluminum (blue) and Copper (green). The hyperspectral projections are then decomposed into material projections. The material projections from different poses are finally fused in a MACE framework to form a joint reconstruction of the material volumes.

demonstrate that multi-pose APMD achieves more accurate material reconstructions compared to APMD from a single pose.

The rest of this paper is organized as follows. First, we present the material projection extraction technique for HS data. Next, we present the multi-pose fusion which uses the material projections as inputs, followed by results on simulated data.

II. Material Projection Extraction

In this step, we estimate material projections, which involves first determining the μ-spectra for all materials using single-pose data and then leveraging these spectra to extract material projections for all poses. To ensure fast and accurate estimation of the material μ-spectra, we adopt the subspace extraction-based approach from [6]. Let K be the number of measurement poses, N_p be the number of CT measurements per pose, N_λ be the number of wavelength bins, and N_m be the number of materials. We define $p_k \in \mathbb{R}^{N_p \times N_\lambda}$ as the hyperspectral projection measurements from the k^{th} pose. The objective is to estimate material projections $V_k \in \mathbb{R}^{N_p \times N_m}$ by approximating $p_k = V_k D^t$, where $D \in \mathbb{R}^{N_\lambda \times N_m}$ is a material basis matrix with each column containing the estimated μ-spectra for a specific material [5] (see Figure 2). The material projections are obtained by solving the NMF problem for all the poses with a fixed D:

$$V_k = \underset{V_k \geq 0}{\arg\min} \left\{ \|p_k - V_k D^t\|^2 \right\}, \quad k = 0, ..., K-1 \qquad (1)$$

These material projections from different poses are then used to form a joint tomographic reconstruction of the underlying materials.

III. Multi-pose Fusion

A. Problem formulation

As illustrated in Figure 1, Multi-pose Fusion takes the material projections from different poses as inputs, and performs a joint reconstruction that fits the projection data from all the poses. Let N_{vox} be the number of voxels of the sample to be recovered. We define $x \in \mathbb{R}^{N_{vox} \times N_m}$ as the image vector containing attenuation coefficients to be recovered in the reconstruction coordinate system. For each pose $k \in \{0, ..., K-1\}$, we also define a transformation function $x_k = T_k x$ where x is the object represented in the common reconstruction coordinate system and x_k is the object represented in the k^{th} pose. T_k transforms the object from the common reconstruction coordinate system to the posed coordinate system. In practice, T_k typically implements a rigid body transformation [10], so it requires that the discretized function be resampled on the transformed sampling grid. This process requires some form of typically spline-based interpolation algorithm [11]. We will also require an approximate inverse transformation T_k^{-1}. Since both transforms require interpolation and resampling, we note that they will not in general be exact inverses of each other.

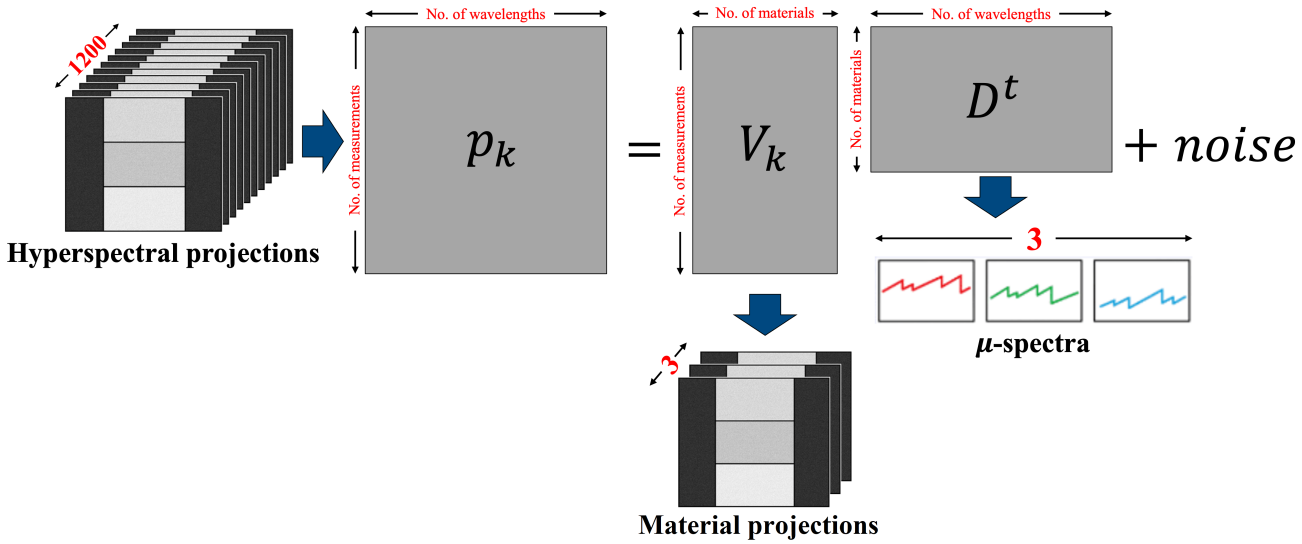

Fig. 2: Overview of material projection extraction. The hyperspectral projections (p_k), in this illustration having 1200 bins, are decomposed into low-dimensional (3 in this illustration) material projections (V_k) using the corresponding material basis vectors (D). The V_k from each pose is used for subsequent multi-pose fusion.

Using this notation, the forward model for each pose has the form

$$V_k = A_k T_k x + w_k \ , \tag{2}$$

where $V_k \in \mathbb{R}^{N_p \times N_m}$ are the material projections, $A_k \in \mathbb{R}^{N_p \times N_{vox}}$ is the scanner system matrix and $w_k \sim N(0, \alpha \Lambda_k^{-1})$ is independent additive noise for the k^{th} pose. The joint MBIR reconstruction for the multi-pose problem is then given by

$$x^* = \arg\min_x \left\{ \sum_{k=0}^{K-1} f_k(x) + h(x) \right\} \tag{3}$$

with data fidelity terms given by

$$f_k(x) = \frac{1}{2} \| V_k - A_k T_k x \|^2_{\Lambda_k} \ , \tag{4}$$

and a regularization term given by $h(x)$. Notice that direct implementation of (3) is difficult since it requires that software be written to minimize a sum of complex tomographic reconstruction terms each with a different transformation T_k. Instead, we propose to find a solution for the HS reconstruction from multiple poses using the MACE [9] framework.

B. MACE formulation of Multi-pose Fusion

In this section, we introduce the MACE framework for solving the multi-pose reconstruction problem [12], [13]. The MACE framework formulates the reconstruction as a consensus solution of multiple competing agents each of which transforms an initial solution to a more desirable solution. The definition of what a more desirable solution means differs - some agents will find solutions that match the measurements better under the appropriate forward model, while others will ensure that any solution to the inverse problem satisfies certain desirable properties such as lying on the mainfold of 3D volumes. We start by describing the agents in our approach. Let $x' = F_k(x)$ be a data-fitting agent for the k^{th} pose. Intuitively, this agent should take a reconstruction x and return a reconstruction x' that better fits the material projections V_k from pose k. One approach would be to use the data-fitting terms from (4) directly in a proximal map. However, this would be computationally expensive and difficult to compute since it requires that the transformation T_k be integrated into the reconstruction software. Alternatively, we propose to use a *conjugate proximal map* given by

$$F_k(w) = T_k^{-1} F(T_k w; V_k) \ , \tag{5}$$

where $F(w; V_k)$ is the standard proximal map in reconstruction coordinates given by

$$F(w; V_k) = \arg\min_x \left\{ \frac{1}{2} \| V_k - A_k x \|^2_{\Lambda_k} + \frac{1}{2\sigma^2} \| x - w \|^2_2 \right\} . \tag{6}$$

Notice that the conjugate proximal map of (5) can be computed easily since it requires only the computation of the standard proximal map of (6) in the standard coordinates and pre- and post-composition with the spline-based maps T_k and T_k^{-1}. In fact, software for computing the proximal map in (6) is openly available [14], [15]. For the prior model, we will use a BM4D denoiser [16]. We denote this agent by F_K.

For notational simplicity, we define the stacked set of agents as

$$\mathbf{F}(\mathbf{w}) = [F_0(w_0), \cdots, F_K(w_K)] \tag{7}$$

where $\mathbf{w}$ is the stacked input vector given by

$$\mathbf{w} = [w_0, \cdots, w_K] \ .$$

We also define an averaging operator

$$\mathbf{G}(\mathbf{w}) = [\bar{w}, \cdots, \bar{w}] \ , \tag{8}$$

where $\bar{w}$ is a weighted average of the input vector components given by

$$\bar{w} = \sum_{k=0}^{K} \mu_k w_k, \tag{9}$$

and μ_k is the weight for each agent, computed as

$$\mu_k = \begin{cases} \frac{1}{K(1+\beta)}, & 0 \le k \le K-1 \\ \frac{\beta}{(1+\beta)}, & k = K \end{cases} .$$

β provides a means to weight the amount of regularization relative to the data-fitting agents. Using this notation, the MACE equilibrium equation is

$$\mathbf{F}(\mathbf{w}) = \mathbf{G}(\mathbf{w}) \ . \tag{10}$$

This equation enforces that all agents have the same output value (consensus) and that the vectors $\delta_k = w_k - F_k(w_k)$ satisfy $\sum_{k=0}^{K} \mu_k \delta_k = 0$ (equilibrium) [12].

C. Computing the MACE Solution

Algorithm 1 MACE Algorithm for Multi-pose Fusion

Input: Initial Reconstruction: $x^{(0)} \in \mathbb{R}^N$
Output: Final Reconstruction: $x^* \in \mathbb{R}^N$

$\mathbf{w} \leftarrow [x^{(0)}, ..., x^{(0)}]$
while not converged **do**
  $\mathbf{x} \leftarrow \mathbf{F}(\mathbf{w})$
  $\mathbf{z} \leftarrow \mathbf{G}(2\mathbf{x} - \mathbf{w})$
  $\mathbf{w} \leftarrow \mathbf{w} + 2\rho(\mathbf{z} - \mathbf{x})$
return $x^* \leftarrow \sum_{k=0}^{K} \mu_k x_k$

It is shown in [12] that the solution to (10) is also the fixed point of the operator $\mathbf{T} = (2\mathbf{G} - I)(2\mathbf{F} - I)$. One popular method of finding such a fixed point is Mann iteration

$$\mathbf{w} \leftarrow (1-\rho)\mathbf{w} + \rho\mathbf{T}\mathbf{w}, \tag{11}$$

where $\rho \in (0, 1)$ controls the convergence speed. Algorithm 1 shows the general method of solving MACE with Mann iterations. The algorithm starts from an initial reconstruction $x^{(0)}$, and uses Mann iterations to find the equilibrium point between the prior and forward model terms. From [12], when the agents F_k are all proximal maps of associated cost functions f_k and h, this equilibrium point is exactly the solution to the optimization problem of (3).

IV. Results

We implemented our multi-pose APMD algorithm and evaluated it on simulated hyperspectral neutron data. Fig. 3 shows the digital phantom used to generate the synthetic hyperspectral measurements. The digital phantom (size $64 \times 64 \times 64$) is formed from nickel (Ni) and copper (Cu) in an aluminum (Al) structure. The phantom is rotated to three different measurement poses (see Figure 4), and the hyperspectral neutron measurements are generated for each pose respectively, using a Poisson noise model and attenuation calculations based on the object geometry and the theoretically known material spectra computed using the Bragg-edge modeling (BEM) library [17].

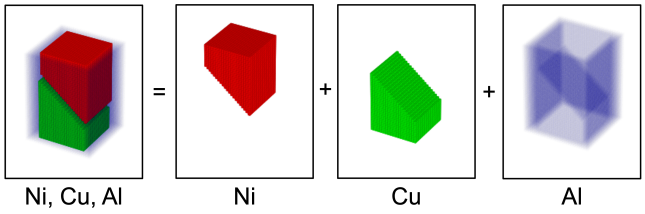

Fig. 3: 3D visualization of the digital phantom. The phantom is composed of three distinct materials: Ni, Cu, Al. The size of the phantom is $64 \times 64 \times 64$

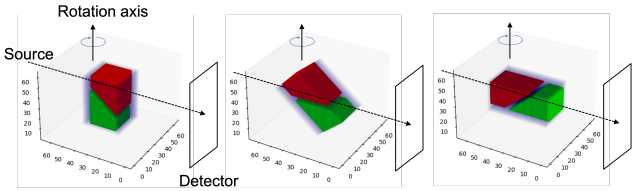

(a). Pose 0 (b). Pose 1 (c). Pose 2

Fig. 4: 3D visualization of the measurement poses. The digital phantom is rotated by 0, 45, 90 degrees respectively. CT measurements are simulated by rotating the phantom at each pose about a single axis from $0 - 180$ degrees. While the data from each pose can be processed as a independent CT data set, we process all the data jointly to produce a single reconstruction.

The multi-pose APMD results are obtained with data from all three poses. Figure 5(a) shows the ground truth slices, Figure 5(b)-(d) shows the APMD results using data from a single pose (rotated to match the orientation of pose 0), and Figure 5(e) shows the multi-pose APMD using data from all three poses. The results indicate that multi-pose APMD results in more accurate material volume reconstructions with reduced noise.

V. Conclusion

In this paper, we introduced a novel autonomous polycrystalline material decomposition (APMD) approach that characterizes and localizes the polycrystalline structures from multiple poses of a single object. The proposed algorithm first decomposes the hyperspectral projection measurements into low-dimensional material projections and then uses MACE to fit the material projections from multiple poses, where the data fidelity from each pose is promoted with a novel MACE agent called a conjugate proximal map. The resulting algorithm has a simple modular implementation using standard CT reconstruction software. Our results on simulated data demonstrate that multi-pose APMD achieves more accurate material reconstructions compared to APMD from a single pose.

References

[1] R. Woracek, D. Penumadu, N. Kardjilov, A. Hilger, M. Boin, J. Banhart, and I. Manke, "3D mapping of crystallographic phase distribution using energy-selective neutron tomography," *Advanced Materials*, vol. 26, no. 24, pp. 4069–4073, 2014.

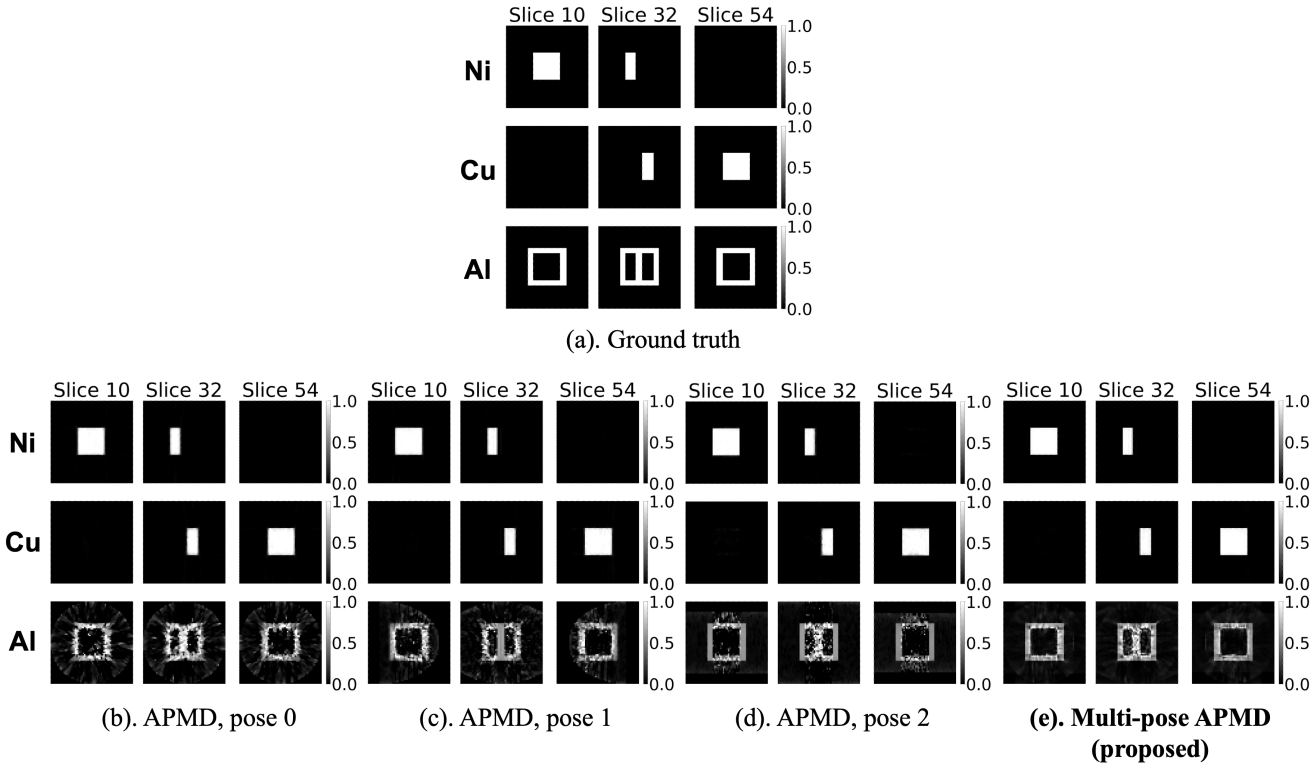

(a). Ground truth

(b). APMD, pose 0 (c). APMD, pose 1 (d). APMD, pose 2 **(e). Multi-pose APMD (proposed)**

Fig. 5: Reconstruction with simulated data: Cross-sections for Ni, Cu, and Al in the space domain: (a) ground truth, (b) estimated by APMD with data from pose 0, (c) estimated by APMD with data from pose 1, (d) estimated by APMD with data from pose 2, (e) estimated by multi-pose APMD with data from poses 0, 1, 2. Notice that the noise in reconstructions from the proposed multi-pose method (e) is lower compared to the single pose algorithms especially in the reconstruction of the Al regions.

[2] T. Balke, A. M. Long, S. C. Vogel, B. Wohlberg, and C. A. Bouman, "Hyperspectral neutron CT with material decomposition," in *IEEE International Conference on Image Processing (ICIP)*, pp. 3482–3486, 2021.

[3] T. Balke, A. M. Long, S. C. Vogel, B. Wohlberg, and C. A. Bouman, "Hyperspectral neutron ct with material decomposition," in *2021 IEEE International Conference on Image Processing (ICIP)*, pp. 3482–3486, IEEE, 2021.

[4] A. S. Losko and S. Vogel, "3d isotope density measurements by energy-resolved neutron imaging," *Scientific Reports*, vol. 12, no. 1, p. 6648, 2022.

[5] E. Ametova, G. Burca, S. Chilingaryan, G. Fardell, J. S. Jørgensen, E. Papoutsellis, E. Pasca, R. Warr, M. Turner, W. R. Lionheart, *et al.*, "Crystalline phase discriminating neutron tomography using advanced reconstruction methods," *Journal of Physics D: Applied Physics*, vol. 54, no. 32, p. 325502, 2021.

[6] M. S. N. Chowdhury, D. Yang, S. Tang, S. V. Venkatakrishnan, H. Z. Bilheux, G. T. Buzzard, and C. A. Bouman, "Autonomous polycrystalline material decomposition for hyperspectral neutron tomography," in *2023 IEEE International Conference on Image Processing (ICIP)*, pp. 1280–1284, IEEE, 2023.

[7] C. Bouman and K. Sauer, "A generalized gaussian image model for edge-preserving map estimation," *IEEE Transactions on image processing*, vol. 2, no. 3, pp. 296–310, 1993.

[8] D. Yang, C. A. Kemp, G. T. Buzzard, and C. A. Bouman, "Multi-pose fusion for sparse-view CT reconstruction using consensus equilibrium," in *2022 58th Annual Allerton Conference on Communication, Control, and Computing (Allerton)*, pp. 1–5, IEEE, 2022.

[9] G. T. Buzzard, S. H. Chan, S. Sreehari, and C. A. Bouman, "Plug-and-play unplugged: Optimization-free reconstruction using consensus equilibrium," *SIAM Journal on Imaging Sciences*, vol. 11, no. 3, pp. 2001–2020, 2018.

[10] D. W. Eggert, A. Lorusso, and R. B. Fisher, "Estimating 3-d rigid body transformations: a comparison of four major algorithms," *Machine vision and applications*, vol. 9, no. 5, pp. 272–290, 1997.

[11] C. De Boor and C. De Boor, *A practical guide to splines*, vol. 27. springer-verlag New York, 1978.

[12] G. T. Buzzard, S. H. Chan, S. Sreehari, and C. A. Bouman, "Plug-and-play unplugged: Optimization-free reconstruction using consensus equilibrium," *SIAM Journal on Imaging Sciences*, vol. 11, no. 3, pp. 2001–2020, 2018.

[13] C. A. Bouman, *Foundations of Computational Imaging: A Model-Based Approach*. Philadelphia: Society for Industrial and Applied Mathematics, 2022.

[14] SVMBIR Development Team, "Super-Voxel Model Based Iterative Reconstruction (SVMBIR)." Software library available from https://github.com/cabouman/svmbir, 2020.

[15] MBIRCONE Development Team, "Model-Based Iterative Reconstruction for cone-beam (MBIRCONE)." Software library available from https://github.com/cabouman/mbircone, 2020.

[16] M. Maggioni, V. Katkovnik, K. Egiazarian, and A. Foi, "Nonlocal transform-domain filter for volumetric data denoising and reconstruction," *IEEE transactions on image processing*, vol. 22, no. 1, pp. 119–133, 2012.

[17] J. Y. Y. Lin and G. Song, "BEM: modeling for neutron Bragg-edge imaging," *Journal of Open Source Software*, vol. 3, no. 30, p. 973, 2018.